# Unified Distributed Control for DC Microgrid Operating Modes

Thomas Morstyn, *Student Member, IEEE,* Branislav Hredzak, *Senior Member, IEEE,* Georgios D. Demetriades, *Member, IEEE,* and Vassilios G. Agelidis, *Senior Member, IEEE*

***Abstract*—This paper proposes a unified distributed control strategy for DC microgrid operating modes, without bus voltage signalling or mode detection mechanisms that are normally required for decentralised control strategies. The proposed control strategy is based on the novel integration of distributed controllers for energy balancing between DC microgrid energy storage systems with distributed controllers used to regulate the average DC microgrid bus voltage, and a new method for controlling the grid connected rectifier that maintains the distributed control structure. Under the proposed control strategy seamless mode transitions are achieved between qualitatively different operating modes, namely, (i) grid connected operation with the rectifier providing load balancing, (ii) grid connected operation with the rectifier charging the energy storage systems and (iii) islanded operation. In all operating modes the average DC microgrid bus voltage is regulated to the microgrid voltage reference, and the energy storage systems are controlled independently of the operating mode to achieve and maintain a balanced energy level. Simulations are presented demonstrating the performance of the proposed control strategy for a 380VDC datacenter with intermittent photovoltaic generation and communication delays expected from a WiFi control network implementation.**

***Index Terms*—DC Microgrid, distributed generation, energy storage, islanding, distributed cooperative control, multi-agent systems.**

## I. Introduction

INCREASINGLY, distributed renewable generation sources are being integrated into power networks to increase energy security, reduce transmission losses, and lower pollution [1]. However, the intermittent nature of renewable generation sources presents challenges for traditional AC power networks, and can reduce power quality and network stability. Linked with the rise of distributed renewable generation sources, such as photovoltaic (PV) and variable speed wind generation, is the proliferation of energy storage (ES) devices and loads with DC power conversion stages [2].

DC microgrids present a means of integrating distributed renewable generation sources and DC loads into power networks, while requiring fewer AC–DC power conversion stages [3]. A DC microgrid is made up of a DC distribution system connecting generation sources, loads and storage devices that can operate as part of the main power network through a grid connected rectifier, or autonomously in islanded mode [4]. An example DC microgrid is shown in Fig. 1. It has been shown that DC microgrids can provide higher reliability than AC microgrids [5], [6]. The lower reliability of AC microgrids is primarily caused by the need for additional AC–DC power stages and switching circuitry to incorporate backup storage devices. High reliability is of particular importance for datacenters, and has motivated the development of the ETSI 380VDC datacenter distribution standards [7].

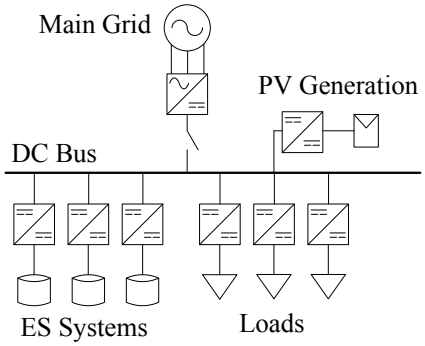


Fig. 1. Example DC microgrid, with loads, ES systems, a PV generation source and a rectifier providing a grid interface.

A DC microgrid has two primary modes of operation, islanded mode and grid connected mode [8]. During islanded mode, power cannot be transferred between the main grid and the DC microgrid, so the demand must be balanced locally. It is desirable to operate intermittent renewable generation sources independently of the microgrid load to provide maximum power point tracking (MPPT) [9]. ES systems, consisting of an ES device and DC-DC converter, can be controlled to absorb or inject power as required to balance the DC microgrid load. Using multiple distributed ES systems, rather than a single central ES system, provides reduced losses and increased reliability [5]. However, a load sharing mechanism is required so that they maintain a balanced energy level. If ES systems prematurely run out of energy they will be unable to use their power capacity to balance fluctuations in microgrid demand [10]. Also, battery ES systems must be kept within certain energy level limits to prevent significant lifetime deterioration [11].

Since the DC voltage varies with the microgrid power balance, V–I droop control can be used to provide load sharing between the ES systems, without requiring communication links [12]. However, V–I droop control requires a steady state voltage offset. Also, an uneven load distribution will lead to

T. Morstyn, B. Hredzak and V. G. Agelidis are with the Australian Energy Research Institute and the School of Electrical Engineering and Telecommunications, University of New South Wales (UNSW Australia), Sydney, NSW 2052 Australia (email: t.morstyn@student.unsw.edu.au, b.hredzak@unsw.edu.au, vassilios.agelidis@unsw.edu.au).

G. D. Demetriades is with ABB Corporate Research, Västerås 721 78, Sweden (email: georgios.demetriades@se.abb.com).

voltage drops across the DC lines and degrade load sharing accuracy [13]. A centralised control system can be used to correct these issues [14].

In grid connected mode it may be desirable for the grid connected rectifier to balance the microgrid load. In this case the DC microgrid acts as an uncontrolled load in the main grid [8]. In this mode the ES systems should only provide transient power injection to improve DC bus voltage regulation, so that they do not run out of energy. Alternatively, it may be desirable to operate the DC microgrid as a controlled AC load with a regulated output power. This allows grid power quality requirements to be enforced. Controlled AC load operation can also be used for ES system charging [15]. Grid connected operation and islanded operation require qualitatively different behaviour from the microgrid terminal devices, and thus coordination between the ES systems and the grid connected rectifier is required.

Decentralised control strategies have been presented that use DC bus voltage signalling to provide coordinated control, without requiring communication links [16], [17]. Under a bus voltage signalling control strategy DC voltage offsets are used to share the information necessary for the DC microgrid terminal devices to cooperatively control the microgrid operating mode. Since DC bus voltage signalling necessitates steady state voltage offsets, the microgrid will operate at different voltage levels depending on the operating mode. In this case additional power conditioning equipment or more expensive transmission infrastructure will be required to connect equipment with a limited voltage operating range, such as ICT equipment [18]. Also, since the DC bus voltage is used to determine the operating mode, voltage disturbances may cause incorrect operation.

A central control system connected to all of the DC microgrid terminal devices can be used to ensure smooth transitions between operating modes [19]. However, a centralised control system introduces a single point of failure and reduces scalability [20].

The limitations inherent in the centralised and decentralised control approaches motivate the application of distributed control. Distributed control strategies allow coordination between autonomous agents, using only neighbour to neighbour communication over a sparse communication network. This provides advantages in terms of robustness, extensibility and flexibility over centralised control strategies [21]. In [22] a distributed control strategy for voltage regulation and load sharing between distributed generators in islanded DC microgrids is presented. However, operating requirements specific to ES systems are not addressed. In [23] low bandwidth communication between distributed generators is used for voltage regulation in islanded DC microgrids, and in [24] a similar communication strategy is used for energy balancing between ES systems. However, these control strategies are not fully distributed, in the sense that each ES system requires information from all other systems in the microgrid, and therefore a fully connected communication network is required. In [25] a distributed control strategy for energy balancing between ES devices in islanded DC microgrids is presented, but without consideration to average bus voltage regulation. Also, grid connected DC microgrid operating modes are not considered in any of these papers.

Distributed control strategies have been proposed for accurate power sharing [26] and voltage regulation [27] in droop controlled AC microgrids. In [10] a distributed control strategy for cooperative frequency regulation and energy balancing between AC microgrid ES systems is presented. The control of f–P droop controlled AC microgrids is in some ways analogous to the control of V–I droop controlled DC microgrids [13]. However, in a DC microgrid the average bus voltage deviation must be corrected while maintaining the relative bus voltage differences to maintain accurate power sharing. In an AC microgrid all buses share the same frequency, so the methods used to correct for frequency deviations in droop controlled AC microgrids cannot be directly used to correct voltage deviations in DC microgrids. Also, the distributed AC microgrid control strategies from [10], [26], [27] do not consider grid connected operation.

This paper proposes a unified distributed control strategy for the operating modes of DC microgrids with variable loads/sources, ES systems and a grid connected rectifier, such as the example shown in Fig. 1. The salient features of the proposed control strategy are as follows.

- Distributed controllers for energy balancing between DC microgrid ES systems are integrated with distributed controllers for regulating the average DC microgrid bus voltage.
- Steady state analysis is provided demonstrating that due to the introduction of the energy balancing controllers, standard distributed PI voltage controllers are no longer able to regulate the average DC microgrid bus voltage. This has been solved by replacing the distributed voltage controllers with double integrator controllers.
- A dynamic saturation constraint for the ES systems ensures they are not overloaded. The saturation constraint prioritises voltage regulation over energy balancing when these control objectives are opposed.
- A novel strategy has been proposed for controlling the grid connected rectifier that provides seamless transitions between DC microgrid operating modes while maintaining a distributed control structure. This is made possible by the distributed control strategy presented in this paper for cooperative bus voltage regulation and energy balancing between DC microgrid ES systems.

The proposed unified distributed control strategy has the following advantages. Using only neighbour to neighbour communication over a sparse communication network, the DC microgrid ES systems cooperate to reach a balanced per-unit energy level, and to regulate the average DC microgrid bus voltage to a desired reference. Once a balanced per-unit energy level is achieved the ES systems maintain it through accurate load sharing. The ES systems operate independently of the microgrid operating mode, without bus voltage signalling or mode detection mechanisms which are normally required by decentralised control strategies. Based on information received from a neighbouring ES system, the grid connected rectifier can set the DC microgrid operating mode by selecting its local

real power reference. Seamless mode transitions are achieved between qualitatively different operating modes, namely (i) grid connected operation with the rectifier providing load balancing, (ii) grid connected operation with the rectifier providing ES system charging and (iii) islanded operation. Table I shows a comparison between the features offered by the proposed control strategy and existing decentralised and distributed DC microgrid control strategies. Simulation results demonstrate the performance of the proposed control strategy for a 380VDC datacenter with intermittent PV generation and communication delays. Results show that the DC microgrid voltage is regulated during all modes and mode transitions while the ES systems achieve and maintain a balanced per-unit energy level.

This paper is organised as follows. Section II describes the proposed unified distributed control strategy. Section III presents a global linear system model and steady state analysis for the microgrid voltage regulation dynamics. Section IV presents simulations demonstrating the performance of the proposed control strategy. Section V concludes the paper.

## II. Unified Distributed Control

The proposed unified distributed control strategy provides coordination between the grid connected rectifier and distributed battery ES systems of a DC microgrid. The ES systems have two control objectives. First, the ES systems should regulate the average DC bus voltage to the microgrid reference. Second, the ES systems should converge to a common per-unit energy level and maintain it through accurate load sharing. The per-unit energy level of each ES system is given by its stored energy divided by its maximum capacity. Balancing the per-unit energy levels allows ES systems of different sizes to be used.

The microgrid power balance must be maintained during all operating modes to achieve bus voltage regulation. During islanded mode the ES systems must provide the full microgrid load to maintain voltage regulation. When the DC microgrid is connected to the main grid, the rectifier output power sets the mode of operation of the DC microgrid. Two grid connected operating modes are considered in this study, load balancing and ES charging. In load balancing mode the rectifier output power matches the microgrid load. In this mode the DC microgrid operates as an uncontrolled load in the main grid. The ES systems inject or absorb power so that they converge to a common per-unit energy level. Once a common per-unit energy level is reached, the ES systems provide only transient power injection to regulate the microgrid bus voltages following generation or demand fluctuations. In ES charging mode the rectifier injects power up to its maximum power capacity to charge the ES systems to a desired per-unit energy level. In this mode the DC microgrid operates as a controlled load in the main grid.

The proposed unified distributed control strategy is based on a sparse communication network allowing the ES systems to share information with their neighbours. Each ES system maintains a local estimate of the average ES system per-unit energy level, average microgrid bus voltage and average ES system output current. These estimates are updated based on local measurements and a distributed average consensus protocol. Having access to the average ES system per-unit energy level and average microgrid bus voltage allows the ES systems to control their output current so that they reach a common per-unit energy level, while maintaining microgrid voltage regulation.

The grid connected rectifier receives estimates of the average ES system per-unit energy level and average ES system output current from a neighbouring ES system. To operate the microgrid in load balancing mode, the rectifier controls its real output power to regulate the average ES system output current to zero. The rectifier uses the average ES system per-unit energy level to operate the microgrid in ES charging mode.

Under the proposed control strategy the DC microgrid grid connected rectifier and ES systems operate as autonomous agents, controlled based on neighbour to neighbour communication over a sparse communication network to achieve cooperative control objectives. This removes the need for a central controller and provides advantages in terms of robustness, extensibility and flexibility inherent in a distributed control structure [21].

### A. Battery Energy Storage Systems

A block diagram of a battery ES system and its control system is shown in Fig. 2. A bidirectional DC–DC boost converter provides a power interface between the battery and the DC microgrid. The V–I droop controller sets the DC–DC converter output voltage reference $v_i^*$ based the microgrid voltage reference $v^{mg}$ and the local output current measurement $i_i$. Under the proposed distributed control strategy, the droop control is modified by a voltage regulation control signal $u_i^{\bar{v}}$ and energy balancing control signal $u_i^e$, which act as droop control current reference signals. The voltage regulation control signal is set to regulate the average DC microgrid bus voltage to the microgrid voltage reference. The energy balancing control signal is set to achieve per-unit energy balancing between the ES systems and to maintain it through accurate load sharing.

$$v_i^* = v^{mg} - F_i r_i (i_i - u_i^{\bar{v}} - u_i^e) \tag{1}$$

Traditional decentralised V–I droop control does not include $u_i^{\bar{v}}$ and $u_i^e$, so the load is shared between the ES systems in inverse proportion with their droop control virtual resistances $r_i$. The virtual resistance is selected so that the ES system will use its full output power capacity $[-P_i^{max},\ P_i^{max}]$ to maintain the microgrid voltage within the maximum deviation $\Delta v$ from the microgrid reference.

$$r_i = \frac{\Delta v}{P_i^{max}/v^{mg}} \tag{2}$$

The DC microgrid is subject to high frequency harmonics due to converter switching. A low pass filter with cut off frequency $\omega_i^c$ is applied to prevent the droop control from varying based on high frequency switching harmonics.

$$F_i = \frac{\omega_i^c}{s + \omega_i^c} \tag{3}$$

TABLE I
COMPARISON WITH DECENTRALISED AND DISTRIBUTED DC MICROGRID CONTROL STRATEGIES

| | [16] | [17] | [22] | [23] | [24] | [25] | This Paper |
|---|---|---|---|---|---|---|---|
| No central controller required | ✓ | ✓ | ✓ | ✓ | ✓ | ✓ | ✓ |
| Only sparse communication required | ✓ | ✓ | ✓ | | | ✓ | ✓ |
| ES system energy levels balanced | | | | | ✓ | ✓ | ✓ |
| Bus voltage signalling not required | | | ✓ | ✓ | | | ✓ |
| Average bus voltage regulated | | | ✓ | ✓ | | | ✓ |
| Grid connected and islanded operation | ✓ | ✓ | | | | | ✓ |

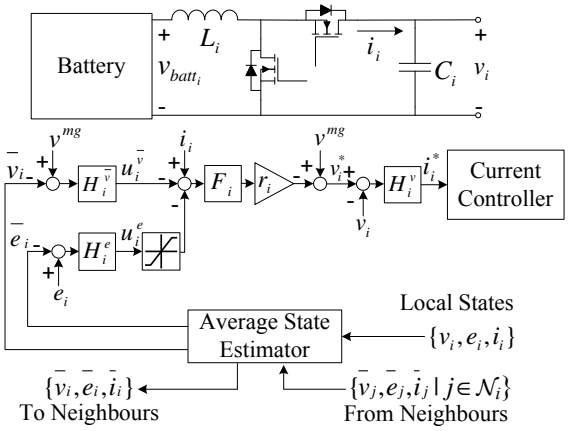


Fig. 2. Battery ES system and control system.

The PI voltage controller $H_i^v$ sets the DC–DC converter current reference to regulate the ES system output voltage to the reference set by the droop controller.

$$i_i^* = H_i^v(v_i^* - v_i), \text{ where } H_i^v = k_i^{vp} + \frac{k_i^{vi}}{s} \tag{4}$$

The current controller sets the duty cycle of the complementary switching of the DC–DC converter MOSFETS to regulate the output current [28].

The PI energy balancing controller $H_i^e$ sets the energy balancing control signal to regulate the ES system per-unit energy level $e_i$ to the local estimate of the average microgrid ES system per-unit energy level $\bar{e}_i$.

$$u_i^e = H_i^e(e_i - \bar{e}_i), \text{ where } H_i^e = k_i^{ep} + \frac{k_i^{ei}}{s} \tag{5}$$

The double integral microgrid voltage controller $H_i^{\bar{v}}$ sets the voltage regulation control signal to regulate the local estimate of the average bus voltage to the microgrid voltage reference.

$$u_i^{\bar{v}} = H_i^{\bar{v}}(v^{mg} - \bar{v}_i), \text{ where } H_i^{\bar{v}} = k_i^{\bar{v}p} + \frac{k_i^{\bar{v}i}}{s} + \frac{k_i^{\bar{v}ii}}{s^2} \tag{6}$$

The double integral gain is required to ensure that the average bus voltage converges to the microgrid voltage reference in steady state, despite the interaction with the energy balancing controller. This is demonstrated in Section III-B through steady state analysis of the global microgrid voltage regulation dynamics.

Due to the energy balancing controller and microgrid voltage controller, the virtual resistance selection from (2) no longer ensures the ES system will not be overloaded. To prevent this, a dynamic saturation constraint is applied to the energy balancing control signal $u_i^e$ to enforce the following constraint.

$$\left| u_i^e + \frac{v^{mg} - v_i}{r_i} + u_i^{\bar{v}} \right| \leq \frac{P_i^{max}}{v_i} \tag{7}$$

Microgrid voltage regulation is prioritised over energy balancing, since voltage regulation is a shorter term goal with direct impact on network stability. Applying the saturation constraint to $u_i^e$, rather than $u_i^e + u_i^{\bar{v}}$, ensures that even in the case of a large energy difference between the ES systems, $u_i^e$ will not crowd out an opposing $u_i^{\bar{v}}$.

### *B. Distributed Average Consensus Protocol*

Each ES system has an average state estimator that uses local measurements and information from neighbouring ES systems to update local estimates of the average ES system per-unit energy level $\bar{e}_i$, average microgrid bus voltage $\bar{v}_i$ and average ES system output current $\bar{i}_i$. The average state estimator implements a distributed average consensus protocol for tracking dynamic signals from [29].

The DC microgrid ES systems are connected by a sparse communication graph $\mathcal{G}(\mathcal{V}, \mathcal{E})$, with nodes $\mathcal{V} = \{1, ..., N\}$ and edges $\mathcal{E}$. Each graph node represents an ES system and the graph edges represent communication links between them. $(i, j) \in \mathcal{E}$ if there is a communication link allowing information flow from node $i$ to node $j$. The neighbours of node $i$ are given by $\mathcal{N}_i$, where $j \in \mathcal{N}_i$ if $(j, i) \in \mathcal{E}$. The graph adjacency matrix is given by $\mathbf{A} = [a_{ij}] \in \mathbb{R}^{N \times N}$, where $a_{ij} > 0$ if $(j, i) \in \mathcal{E}$ and $a_{ij} = 0$ otherwise.

For the $i$th ES system let $x_i$ be a local state variable, and let $\bar{x}_i$ be the local estimate of the average value of that state for the microgrid ES systems. The $i$th ES system receives average state estimates from its neighbours $j \in \mathcal{N}_i$, and its average state estimator implements the following distributed average consensus protocol.

$$\bar{x}_i = x_i + \int \sum_{j \in \mathcal{N}_i} a_{ij}(\bar{x}_j - \bar{x}_i)dt \tag{8}$$

Each node in the communication network has in-degree $d_i = \sum_{j=1}^{N} a_{ij}$ and out-degree $d_i^o = \sum_{j=1}^{N} a_{ji}$. The graph is balanced if $d_i = d_i^o$ for all nodes. The graph degree matrix

is given by $\mathbf{D} = \text{diag}\{d_i\}$ and the graph Laplacian matrix is given by $\mathbf{L} = \mathbf{D} - \mathbf{A}$.

The global dynamics of the distributed average consensus protocol are given by

$$\dot{\bar{\mathbf{x}}} = \dot{\mathbf{x}} - \mathbf{L}\bar{\mathbf{x}}, \text{ where } \bar{\mathbf{x}} = \begin{bmatrix}\bar{x}_1 & \bar{x}_2 & \cdots & \bar{x}_N\end{bmatrix}^T \quad (9)$$

$$\mathbf{x} = \begin{bmatrix}x_1 & x_2 & \cdots & x_N\end{bmatrix}^T. \quad (10)$$

Applying the Laplace transform yields the following transfer function matrix for the distributed average consensus protocol [29].

$$\mathbf{H}^{avg} = \frac{\bar{\mathbf{X}}}{\mathbf{X}} = s(s\mathbf{I}_N + \mathbf{L})^{-1} \quad (11)$$

$\bar{\mathbf{X}}$ and $\mathbf{X}$ are the Laplace transforms of $\bar{\mathbf{x}}$ and $\mathbf{x}$ respectively, and $\mathbf{I}_N \in \mathbb{R}^{N\times N}$ is the identity matrix.

For a balanced communication graph with a spanning tree, the steady state gain of the distributed average consensus protocol is given by the averaging matrix $\mathbf{Q}$ [22].

$$\lim_{s\to 0} \mathbf{H}^{avg} = \mathbf{Q}, \text{ where } [\mathbf{Q}]_{ij} = 1/N. \quad (12)$$

The final value theorem shows that for a vector of step inputs $\mathbf{x}$, the elements of $\bar{\mathbf{x}}$ converge to the global average of the steady state values, $\langle \mathbf{x}^{ss} \rangle$.

$$\lim_{t\to\infty} \bar{\mathbf{x}}(t) = \lim_{s\to 0} \mathbf{H}^{avg} \lim_{s\to 0} s\mathbf{X} = \mathbf{Q}\mathbf{x}^{ss} = \langle \mathbf{x}^{ss} \rangle \underline{\mathbf{1}} \quad (13)$$

Actual communication technologies will introduce communication delays between the ES systems. For instance, for WiFi communication, processing, encapsulation, decapsulation and propagation delays are expected [30]. Let $\tau_{ij}$ be the delay for communication link $(j, i)$. In this case the distributed average consensus protocol dynamics can be expressed as

$$\bar{x}_i(t) = x_i(t) + \int \sum_{j\in\mathcal{N}_i} a_{ij}(\bar{x}_j(t-\tau_{ij}) - \bar{x}_i(t-\tau_{ij}))dt. \quad (14)$$

The stability of the distributed average consensus protocol is sensitive to time delays. In [31] it is shown that for uniform communication link delays $\tau_{ij} = \tau$, the distributed average consensus protocol solves the average consensus problem if and only if $\tau < \pi/2\lambda_N$, where $\lambda_N$ is the largest eigenvalue of the graph Laplacian matrix $\mathbf{L}$.

Selection of the communication network link weights $a_{ij}$ presents a trade-off between convergence speed and robustness to communication delays. This trade-off is analysed in [31]. Higher link weights increase the speed with which the ES systems approach consensus, so that their estimates of the average microgrid bus voltage, average output current and average ES system energy level are near the actual average values of these quantities. However, higher link weights also increase $\lambda_N$ and thus reduce the maximum acceptable communication link delay. In this study all link weights are selected to be $a_{ij} = 1$.

### C. Grid Connected Rectifier

A three phase four quadrant voltage source rectifier provides power transfer between the DC microgrid and the main grid. A block diagram of the rectifier and its control system is shown in Fig. 3. When the DC microgrid is connected to the main grid, the rectifier real output power is controlled to achieve the desired DC microgrid operating mode and the reactive output power is controlled to provide voltage support to the PCC with the main grid. This is achieved using decoupled d–q axis direct power current control [32]. An LC output filter provides the required attenuation of output voltage harmonics to meet utility requirements [33].

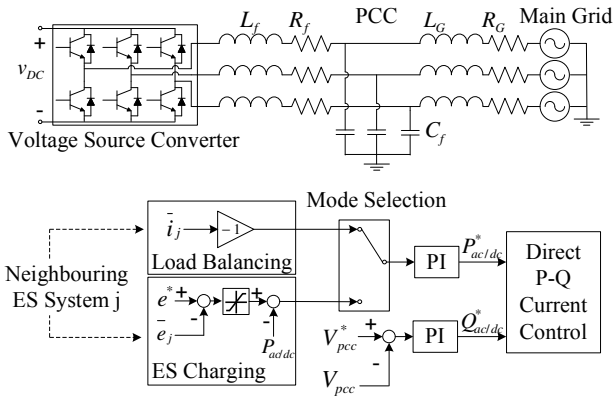


Fig. 3. Grid connected rectifier and control system.

The rectifier receives estimates of the average ES system output current and average ES system per-unit energy level from a neighbouring ES system in the communication network. In load balancing mode the rectifier real power reference is set by a PI controller to regulate the average ES system output current estimate $\bar{i}_j$ to zero. In ES charging mode the rectifier real power reference is set to regulate the average ES system per-unit energy level estimate $\bar{e}_j$ to a per-unit energy level reference $e^*$. A saturation constraint is applied to the real power reference so that the rectifier real power capacity $[-P^{max}_{ac/dc}, P^{max}_{ac/dc}]$ is not violated.

The DC microgrid reactive power is controlled to provide voltage support to the PCC with the main grid, using a control strategy for battery connected STATCOM [34]. A PI controller sets the reactive power reference to regulate the magnitude of the PCC voltage $V_{pcc}$ to the main grid voltage reference $V^*_{pcc}$.

In this study it assumed that the main grid feeds the AC side of the rectifier. However, the only requirement for operating the DC microgrid in load balancing and ES charging mode is an AC network that allows the rectifier real output power to be directly controlled. Therefore, for additional reliability a controllable power source such as a diesel generator could be connected to the AC side of the rectifier. In this case the DC microgrid could still be operated in load balancing or ES charging mode without a connection to the main grid.

## III. Global Microgrid Modelling

Neglecting non-linear dynamics and saturation constraints, the global DC microgrid voltage regulation dynamics can be modelled by a multiple output linear system which takes the microgrid voltage reference as the input and gives the microgrid bus voltages as outputs. Based on this linear system model the ES system microgrid voltage controllers $H^{\bar{v}}_i$,

energy balancing controllers $H_i^e$ and communication network Laplacian matrix $\mathbf{L}$ can be designed to provide stability and a desirable transient response. Steady state analysis is carried out to demonstrate that the average DC microgrid bus voltage converges to the microgrid voltage reference.

### A. Global Dynamic Modelling

Let $V^{mg}$ be the Laplace transform of the microgrid voltage reference. The following Laplace transforms are defined for the global microgrid state vectors.

$$\begin{aligned}
\mathbf{V}^* &= \mathcal{L}\{\mathbf{v}^*\}, \ \mathbf{v}^* = [v_1^* \ v_2^* \ \cdots \ v_N^*]^T \\
\bar{\mathbf{V}} &= \mathcal{L}\{\bar{\mathbf{v}}\}, \quad \bar{\mathbf{v}} = [\bar{v}_1 \ \bar{v}_2 \ \cdots \ \bar{v}_N]^T \\
\mathbf{V} &= \mathcal{L}\{\mathbf{v}\}, \quad \mathbf{v} = [v_1 \ v_2 \ \cdots \ v_N]^T \\
\bar{\mathbf{E}} &= \mathcal{L}\{\bar{\mathbf{e}}\}, \quad \bar{\mathbf{e}} = [\bar{e}_1 \ \bar{e}_2 \ \cdots \ \bar{e}_N]^T \\
\mathbf{E} &= \mathcal{L}\{\mathbf{e}\}, \quad \mathbf{e} = [e_1 \ e_2 \ \cdots \ e_N]^T \\
\mathbf{I} &= \mathcal{L}\{\mathbf{i}\}, \quad \mathbf{i} = [i_1 \ i_2 \ \cdots \ i_N]^T
\end{aligned}$$

From (1), the global droop control dynamics are given by

$$\mathbf{V}^* = V^{mg}\underline{\mathbf{1}} - \mathbf{Fr}(\mathbf{I} - \mathbf{H}^{\bar{v}}(V^{mg}\underline{\mathbf{1}} - \bar{\mathbf{V}}) - \mathbf{H}^e(\mathbf{E} - \bar{\mathbf{E}})), \quad (15)$$

$$\text{where } \mathbf{F} = \text{diag}\{F_i\}, \ \mathbf{r} = \text{diag}\{r_i\},$$

$$\mathbf{H}^{\bar{v}} = \text{diag}\{H_i^{\bar{v}}\} \text{ and } \mathbf{H}^e = \text{diag}\{H_i^e\}.$$

Using the distributed average consensus protocol transfer function matrix (11) the global dynamics of the average voltage estimates and per-unit energy level estimates are given by

$$\bar{\mathbf{V}} = \mathbf{H}^{avg}\mathbf{V} \text{ and } \bar{\mathbf{E}} = \mathbf{H}^{avg}\mathbf{E}. \quad (16)$$

The grid connected rectifier, constant power loads and generation sources operating under MPPT act as positive or negative power sources in the DC microgrid, while the ES systems act as bus voltage regulation units. To formulate the bus voltage regulation dynamics, power sources can be modelled by a parallel current source and resistance [35].

Modern DC–DC converters have high switching frequency and current control with delay on the order of one switching period $T_s$. For the purpose of outer loop control design the closed loop bus voltage regulation dynamics between the ES system output voltage reference $v_i^*$ and local bus voltage $v_i$ can be modelled by the following transfer function [36].

$$G_i^{v_{cl}} = \frac{G_i^{v_{ol}}}{1 + G_i^{v_{ol}}}, \text{ where } G_i^{v_{ol}} = \frac{H_i^v}{sC_i(T_s s + 1)} \quad (17)$$

Therefore, the microgrid closed loop local bus voltage regulation dynamics are given by

$$\mathbf{V} = \mathbf{G}^{v_{cl}}\mathbf{V}^*, \text{ where } \mathbf{G}^{v_{cl}} = \text{diag}\{G_i^{v_{cl}}\}. \quad (18)$$

The ES system output currents and bus voltages are related by the bus admittance matrix $\mathbf{Y}$, which is constructed based on the DC microgrid line and load impedances.

$$\mathbf{I} = \mathbf{YV} \quad (19)$$

The following first order model from [11] is used for the battery per-unit energy level dynamics.

$$\dot{e}_i = -\frac{v_i i_i}{e_i^{max}} \quad (20)$$

$e_i^{max}$ is the maximum energy capacity of the $i$th ES system. The energy level dynamics are linearised around the steady state microgrid operating point $v^{mg}\underline{\mathbf{1}}$ at which the ES system output currents are zero. The global energy level dynamics can be modelled by

$$\mathbf{E} = \mathbf{MYV}, \text{ where } \mathbf{M} = \text{diag}\left\{-\frac{v^{mg}}{e_i^{max} s}\right\}. \quad (21)$$

The following multiple output linear system describes the global closed loop DC microgrid voltage regulation dynamics.

$$\begin{aligned}
\mathbf{V} = [&(\mathbf{G}^{v_{cl}})^{-1} + \mathbf{FrY} + \mathbf{FrH}^{\bar{v}}\mathbf{H}^{avg} \\
&- \mathbf{FrH}^e(\mathbf{I}_N - \mathbf{H}^{avg})\mathbf{MY}]^{-1} V^{mg}(\mathbf{I}_N + \mathbf{FrH}^{\bar{v}})\underline{\mathbf{1}} \quad (22)
\end{aligned}$$

### B. Steady State Analysis

Let $v^{mg}$ be the microgrid voltage reference. In this case the input to the global closed loop microgrid voltage regulation dynamics is given by

$$V^{mg} = \frac{v^{mg}}{s}. \quad (23)$$

The steady state DC microgrid bus voltages are obtained by applying the final value theorem to (22).

$$\begin{aligned}
\mathbf{v}^{ss} &= \lim_{s\to 0} s\mathbf{V} \quad (24) \\
&= \lim_{s\to 0}[s^2(\mathbf{G}^{v_{cl}})^{-1} + s^2\mathbf{FrY} + s^2\mathbf{FrH}^{\bar{v}}\mathbf{H}^{avg} \\
&\quad - s^2\mathbf{FrH}^e(\mathbf{I}_N - \mathbf{H}^{avg})\mathbf{MY}]^{-1} s^2 v^{mg}(\mathbf{I}_N + \mathbf{FrH}^{\bar{v}})\underline{\mathbf{1}}
\end{aligned}$$

The steady state bus voltages can be obtained based on the following limits.

$$\begin{aligned}
&\lim_{s\to 0} s^2\mathbf{H}^{\bar{v}} = \mathbf{H}^{\bar{v}ii}, \text{ where } \mathbf{H}^{\bar{v}ii} = \text{diag}\{k_i^{\bar{v}ii}\} \quad (25) \\
&\lim_{s\to 0} s\mathbf{H}^e = \mathbf{H}^{ei}, \quad \text{where } \mathbf{H}^{ei} = \text{diag}\{k_i^{ei}\} \\
&\lim_{s\to 0} s\mathbf{M} = \mathbf{M}_0, \quad \text{where } \mathbf{M}_0 = \text{diag}\{-v^{mg}/e_i^{max}\} \\
&\lim_{s\to 0} \mathbf{H}^{avg} = \mathbf{Q}, \ \lim_{s\to 0} \mathbf{Y} = \mathbf{Y}_0, \ \lim_{s\to 0} \mathbf{F} = \mathbf{I}_N, \\
&\text{and} \quad \lim_{s\to 0} (\mathbf{G}^{v_{cl}})^{-1} = \mathbf{I}_N.
\end{aligned}$$

Therefore,

$$\begin{aligned}
\mathbf{v}^{ss} = &[\mathbf{r}(\mathbf{H}^{\bar{v}ii}\mathbf{Q} - \mathbf{H}^{ei}(\mathbf{I}_N - \mathbf{Q})\mathbf{M}_0\mathbf{Y}_0)]^{-1} \\
&v^{mg}(\mathbf{rH}^{\bar{v}ii})\underline{\mathbf{1}} \quad (26)
\end{aligned}$$

which yields,

$$\begin{aligned}
[(\mathbf{H}^{ei})^{-1}\mathbf{H}^{\bar{v}ii}\mathbf{Q} - (\mathbf{I}_N - \mathbf{Q})\mathbf{M}_0\mathbf{Y}_0]\mathbf{v}^{ss} = \\
v^{mg}(\mathbf{H}^{ei})^{-1}\mathbf{H}^{\bar{v}ii}\underline{\mathbf{1}}. \quad (27)
\end{aligned}$$

As shown in (25), without the voltage controller double integral gain the steady state response would be dominated by the energy balancing control. To verify that the average steady state DC microgrid voltage is equal to the microgrid voltage reference, multiply each side of (27) by the averaging matrix $\mathbf{Q}$. Since the column sums of $(\mathbf{I}_N - \mathbf{Q})$ are equal to zero, $\mathbf{Q}(\mathbf{I}_N - \mathbf{Q}) = 0_{N\times N}$. From (13),

$$\begin{aligned}
\mathbf{Q}\left((\mathbf{H}^{ei})^{-1}\mathbf{H}^{\bar{v}ii}\mathbf{Q}\mathbf{v}^{ss}\right) &= v^{mg}\mathbf{Q}\left((\mathbf{H}^{ei})^{-1}\mathbf{H}^{\bar{v}ii}\underline{\mathbf{1}}\right) \quad (28) \\
\langle\mathbf{v}^{ss}\rangle\left\langle(\mathbf{H}^{ei})^{-1}\mathbf{H}^{\bar{v}ii}\underline{\mathbf{1}}\right\rangle\underline{\mathbf{1}} &= v^{mg}\left\langle(\mathbf{H}^{ei})^{-1}\mathbf{H}^{\bar{v}ii}\underline{\mathbf{1}}\right\rangle\underline{\mathbf{1}} \\
\langle\mathbf{v}^{ss}\rangle &= v^{mg}.
\end{aligned}$$

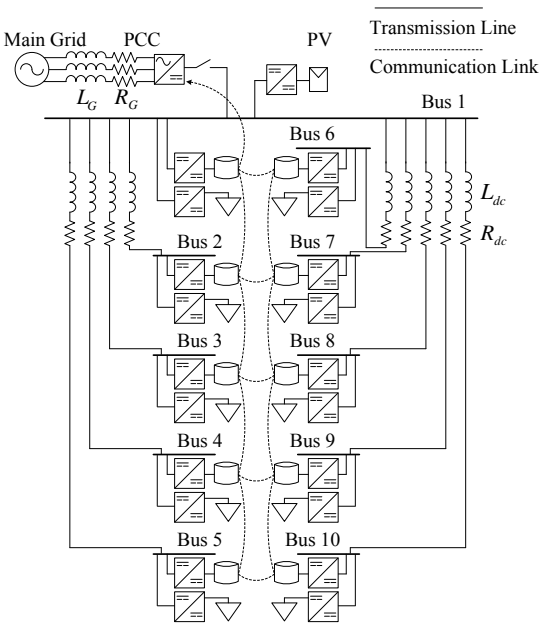


Fig. 4. Case study 10 bus 380VDC datacenter microgrid.

## IV. Case Study

Case study simulations have been carried out in MATLAB/Simulink demonstrating the performance of the proposed unified distributed control strategy for a 380VDC datacenter microgrid. The case studies show the transition from decentralised droop control to the unified distributed control strategy, grid connected operation with the microgrid rectifier operated for load balancing and subsequently for ES system charging and finally a transition to islanded operation after sudden disconnection of the grid connected rectifier. Case Study A includes 20ms communication link delays typical for a WiFi control network implementation [30]. Case Study B demonstrates the performance of the proposed control strategy for the maximum acceptable communication delay of 280ms.

### A. Case Study Microgrid

The datacenter microgrid used for the case studies is shown in Fig. 4. The DC datacenter includes a 10 bus distribution system with PV generation and 10 battery ES systems.

At bus 1, a four quadrant 150kW rated rectifier provides a grid interface. Bus 1 also includes 500m$^2$ PV generation operated for MPPT, rated for 80kW at STC (16% conversion efficiency). Based on the analysis of typical DC datacenter wiring configurations presented in [37], 50m 24mm$^2$ CU cables are selected to connect the load buses to bus 1. Each bus incorporates a 30kW rated battery ES system. The bus 1 to 7 ES systems have 25kWh lithium ion batteries, while the bus 8 to 10 ES systems have 12.5kWh lithium ion batteries. The battery ES systems are connected by a sparse communication network to support the distributed control strategy. The communication links between the ES systems are bidirectional, meeting the distributed control strategy's requirement for a balanced communication network. The bus 1 battery ES system is connected to the grid connected rectifier and provides the rectifier with estimates of the average ES system energy level and average ES system output current. Based on the ETSI EN 300 132-3-1 telecommunications DC distribution standard the datacenter voltage limits are defined as 360V to 400V (380V$\pm 5\%$) [7].

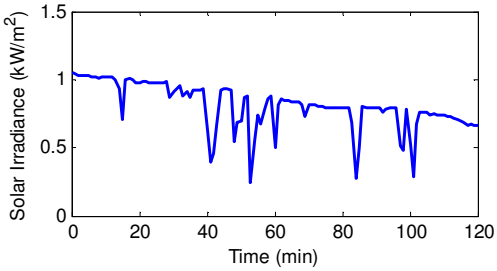


Fig. 5. Case study solar irradiance data.

The rectifier ES charging mode per-unit energy level reference is set to 0.8 (20kWh for the 25kWh ES systems, and 10kWh for the 12.5kWh ES systems). This ensures that if the DC microgrid becomes islanded the ES systems have spare capacity so that they will not empty in the case of excess demand and will not become overcharged in the case of excess supply.

For the case study, buses 1 to 5 are assigned 15kW constant power loads and buses 6 to 10 are assigned 5kW constant power loads, so that the total microgrid load is 100kW. The battery ES systems begin with energy levels between 6kWh and 20kWh. The bus 1 PV generation with MPPT was simulated based on the modelling approach from [38], using one minute resolution irradiance and temperature data for 2pm to 4pm on June 1st 2014 from the NREL Solar Radiation Research Laboratory Baseline Measurement System in Colorado. The irradiance data is shown in Fig. 5. Simulation parameters are provided in Table II.

### B. Case Study A. 20ms Communication Link Delays

The DC microgrid's operation over the full case study simulation time is shown in Fig. 6. The two hour case study can be divided into four periods of operation.

*1) Decentralised V–I droop control; islanded operation, 0min to 10min:* The DC microgrid begins in islanded mode without the proposed unified distributed control strategy. Load sharing between the ES systems is provided without communication by V–I droop control. However, voltage drops between the ES systems leads to inaccurate load sharing. As shown in Fig. 6(a), the energy level of the ES systems at buses 2 to 5 decrease more quickly that the other ES systems since these buses have higher loads, and are not connected to PV generation. Inaccurate load sharing will cause the ES system energy levels to diverge, and cause some to prematurely run out of energy. This is undesirable since exhausted ES systems can no longer contribute their power capacity to voltage regulation. Also, the average DC microgrid bus voltage is below the microgrid voltage reference of 380V, as shown in Fig. 6(c).

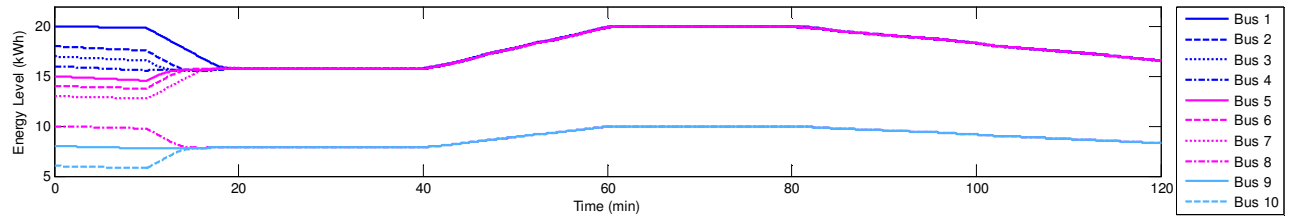


(a) Case Study A. Battery ES system energy levels.

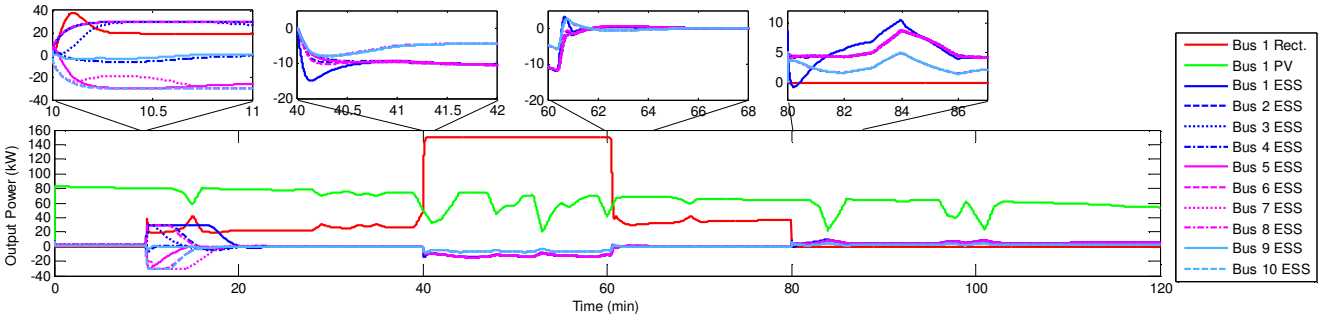


(b) Case Study A. DC microgrid terminal device output powers.

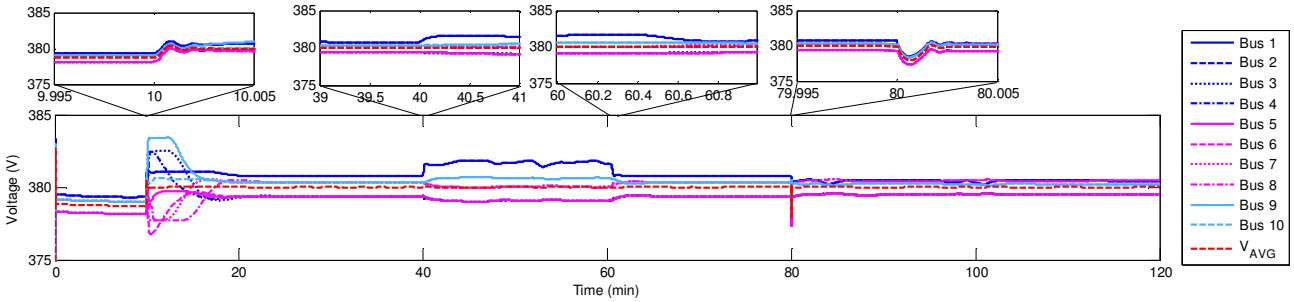


(c) Case Study A. DC microgrid bus voltages.

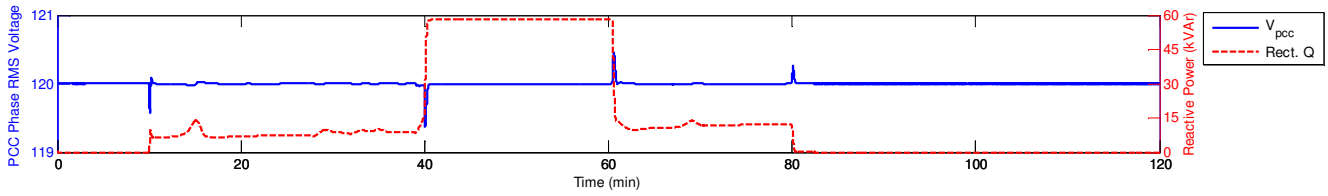


(d) Case Study A. AC RMS voltage magnitude at the main grid PCC (left axis) and grid connected rectifier reactive output power (right axis).

Fig. 6. Case Study A. 380VDC datacenter microgrid with 20ms communication delays. From 0min to 10min, decentralised V–I droop control during islanded operation. From 10min to 40min, grid connected operation with rectifier providing load balancing under the unified distributed control strategy. From 40min to 80min, grid connected operation with rectifier providing ES system charging. From 80min to 120min, islanded operation under the unified distributed control strategy following sudden disconnection of the grid connected rectifier.

*2) Unified Distributed Control; grid connected operation with rectifier providing load balancing, 10min to 40min:* At 10 minutes the unified distributed control strategy is started. Simultaneously, a grid connection is made with the rectifier in load balancing mode. The ES systems use their 30kW power capacity to reach a balanced per-unit energy level, as shown in Fig. 6(b). A per-unit energy level of 0.63 is reached by all of the ES systems (15.74kWh for the 25kWh ES systems at buses 1 to 7 and 7.87kWh for the 12.5kWh ES systems at buses 8 to 10). The ES system microgrid voltage controllers limit the DC microgrid bus voltages between 376.8V and 383.4V ($\pm 0.9\%$ error), and ensure that the average microgrid bus voltage remains at the microgrid voltage reference, as shown in Fig. 6(c). Since the rectifier is operated in load balancing mode, the rectifier transfers power from the main grid to regulate the estimated average ES system output current to zero. As desired, the average ES system per-unit energy level remains constant.

*3) Unified Distributed Control; grid connected operation with rectifier providing ES charging, 40min to 80min:* At 40 minutes the rectifier operating mode is changed from load balancing to ES charging. The rectifier uses its maximum power capacity of 150kW to raise the average ES system per-unit energy level to the 0.8 reference, as shown in Fig. 6(b).

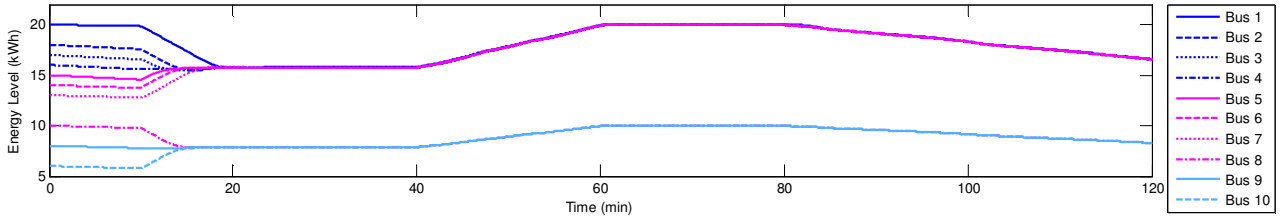


(a) Case Study B. Battery ES system energy levels.

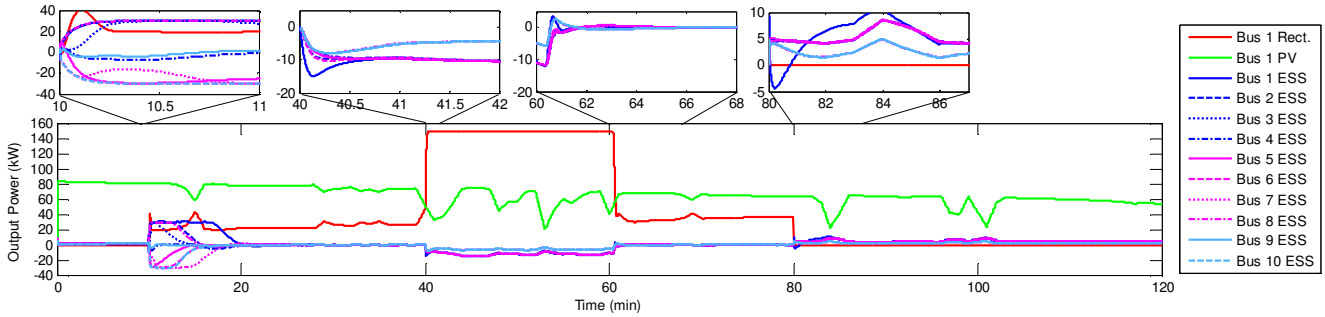


(b) Case Study B. DC microgrid terminal device output powers.

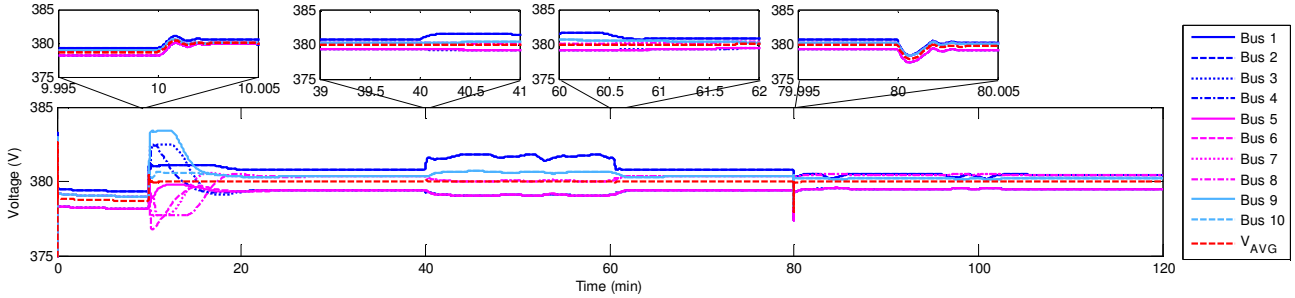


(c) Case Study B. DC microgrid bus voltages.

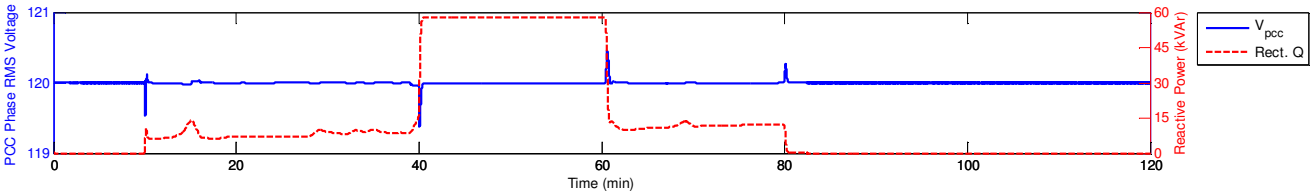


(d) Case Study B. AC RMS voltage magnitude at the main grid PCC (left axis) and grid connected rectifier reactive output power (right axis).

Fig. 7. Case Study B. 380VDC datacenter microgrid with 280ms communication delays. From 0min to 10min, decentralised V–I droop control during islanded operation. From 10min to 40min, grid connected operation with rectifier providing load balancing under the unified distributed control strategy. From 40min to 80min, grid connected operation with rectifier providing ES system charging. From 80min to 120min, islanded operation under the unified distributed control strategy following sudden disconnection of the grid connected rectifier.

The rectifier's reactive power capacity is used to provide voltage support to the PCC with the AC main grid, as shown in Fig. 6(d). Per-unit energy balancing is maintained between the ES systems. The 25kWh ES systems are charged at a common rate and the 12.5kWh ES systems are charged at half this rate. As the ES systems are charged they adjust their output powers to balance the variable PV generation and regulate the average DC microgrid voltage within 0.05V of the 380V microgrid reference, as shown in Fig. 6(c). Once the ES systems reach the 0.8 per-unit ES system reference energy level, the grid connected rectifier reduces its output power so that it matches the microgrid load and the ES system output powers return to zero.

*4) Unified Distributed Control; islanded operation, 80min to 120min:* At 80 minutes the grid connected rectifier is suddenly disconnected, initiating islanded operation. The sudden power imbalance causes the DC microgrid bus voltages to fall, with a minimum level of 377.4V reached. The ES systems react to the fall in voltage by increasing their output powers, restoring the microgrid load balance and returning the average bus voltage to the microgrid reference.

TABLE II
SIMULATION PARAMETERS

| | | | | | |
|---|---|---|---|---|---|
| **Main Grid and DC Microgrid** | | | | | |
| $V^*_{pcc}$ | 120 $V^{RMS}_{phase}$ | $L_G$ | 0.1 mH | $R_G$ | 10 mΩ |
| $v^{mg}$ | 380 VDC | $L_{dc}$ | 7 $\mu H$ | $R_{dc}$ | 36 mΩ |
| **Grid Connected rectifier** | | | | | |
| $e^*$ | 0.8 | $P^{max}_{ac/dc}$ | 150 kW | $f_s$ | 10 kHz |
| $C_f$ | 100 $\mu F$ | $L_f$ | 50 $\mu H$ | $R_f$ | 50 mΩ |
| $k^{P^*p}_{ac/dc}$ | $1\times10^2$ | $k^{P^*i}_{ac/dc}$ | $1\times10^3$ | $k^{Q^*p}_{ac/dc}$ | $1\times10^1$ |
| $k^{Q^*i}_{ac/dc}$ | $1\times10^1$ | | | | |
| **Battery ES Systems** | | | | | |
| $P^{max}$ | 30 kW | $f_s$ | 16 kHz | $v_{batt}$ | 48 V |
| $r$ | 0.2533 | $C$ | 68 mF | $L$ | 80 $\mu H$ |
| $k^{vp}$ | $1\times10^1$ | $k^{vi}$ | $1\times10^1$ | $\omega^c$ | 100 rad/s |
| $k^{ep}$ | $5\times10^3$ | $k^{ei}$ | $5\times10^1$ | $k^{\bar{v}p}$ | $5\times10^2$ |
| $k^{\bar{v}i}$ | $1\times10^1$ | $k^{\bar{v}ii}$ | $1\times10^{-1}$ | | |

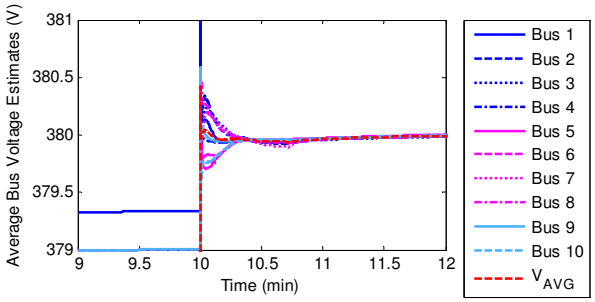


Fig. 8. Case Study A. ES system bus voltage estimates following the start of the distributed average consensus protocol at 10min with 20ms communication link delays.

### C. Case Study B. 280ms Communication Link Delays

With communication link weights $a_{ij} = 1$ the maximum eigenvalue of the graph Laplacian matrix $\mathbf{L}$ is $\lambda_{10} = 5.57$. The theoretical maximum communication link delay for which the distributed average consensus protocol is stable is 282ms [31]. As shown in Fig. 7 the performance of the proposed control strategy with 280ms communication link delays is comparable to the performance with 20ms communication link delays. Fig. 8 and Fig. 9 show the bus voltage estimates following the start of the distributed average consensus protocol 10 minutes into Case Study A and B respectively. The additional communication delay in Case Study B introduces significant oscillatory behaviour into the voltage estimates before they converge to the actual average bus voltage after approximately one minute. Fig. 10 shows that, as expected, for communication link delays of 285ms the ES system average bus voltage estimates do not converge.

## V. CONCLUSION

A unified distributed control strategy for different DC microgrid operating modes has been proposed. The proposed control strategy is based on the novel integration of distributed controllers for energy balancing between ES systems with distributed controllers used to regulate the average DC microgrid bus voltage, and a new method for controlling the

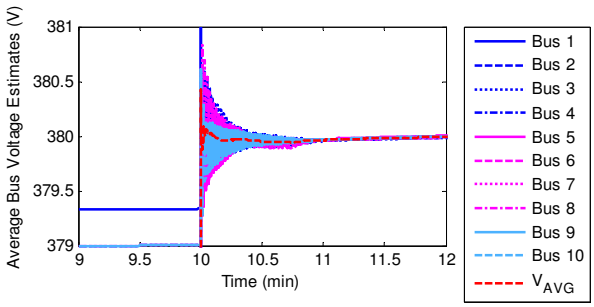


Fig. 9. Case Study B. ES system bus voltage estimates following the start of the distributed average consensus protocol at 10min with 280ms communication link delays.

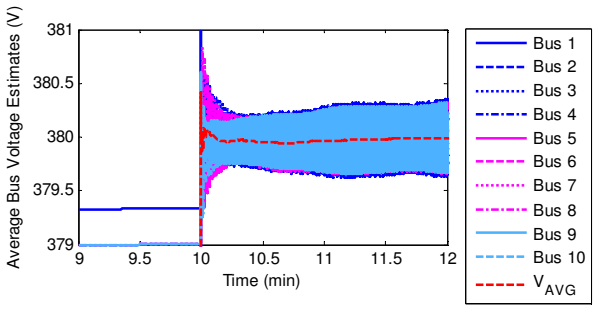


Fig. 10. ES system bus voltage estimates following the start of the distributed average consensus protocol at 10min with 285ms communication link delays. As expected the average bus voltage estimates do not converge in this case.

grid connected rectifier that maintains the distributed control structure. The distributed control structure offers advantages in terms of robustness, extensibility and flexibility over centralised control strategies, since only a sparse communication network is required between the energy storage systems and grid connected rectifier. The main advantages of the proposed control strategy are that the average DC microgrid bus voltage is regulated during all modes and mode transitions and the energy storage systems achieve a balanced energy level and maintain it through accurate load sharing, independently of the operating mode. Simulations have been carried out demonstrating the performance of the proposed control strategy for a 380VDC datacenter with intermittent renewable generation and communication delays expected from a WiFi control network implementation. Promising directions for future work include the extension of the proposed control concept to DC microgrids with a mix of different storage device technologies, and detailed investigation into the implementation of the communications network.

## REFERENCES

[1] P. Mitra, G. T. Heydt, and V. Vittal, "The impact of distributed photovoltaic generation on residential distribution systems," in *2012 North American Power Symposium (NAPS)*, Sep. 2012, pp. 1–6.

[2] N. Eghtedarpour and E. Farjah, "Distributed charge/discharge control of energy storages in a renewable-energy-based DC micro-grid," *IET Renewable Power Generation*, vol. 8, no. 1, pp. 45–57, Jan. 2014.

[3] X. She, S. Lukic, and Q. H. Alex, "DC zonal micro-grid architecture and control," in *IECON 2010 - 36th Annual Conference on IEEE Industrial Electronics Society*, Nov. 2010, pp. 2988–2993.

[4] R. Lasseter, "MicroGrids," in *2002 IEEE Power Engineering Society Winter Meeting. Conference Proceedings (Cat. No.02CH37309)*, vol. 1, 2002, pp. 305–308.

[5] A. Kwasinski, "Quantitative Evaluation of DC Microgrids Availability: Effects of System Architecture and Converter Topology Design Choices," *IEEE Transactions on Power Electronics*, vol. 26, no. 3, pp. 835–851, Mar. 2011.

[6] D. Talapko, "Telecom datacenter power infrastructure availability comparison of DC and AC UPS," *Intelec 2012*, pp. 1–5, Sep. 2012.

[7] D. J. Becker and B. Sonnenberg, "DC microgrids in buildings and data centers," *2011 IEEE 33rd International Telecommunications Energy Conference (INTELEC)*, pp. 1–7, Oct. 2011.

[8] J. J. Justo, F. Mwasilu, J. Lee, and J.-W. Jung, "AC-microgrids versus DC-microgrids with distributed energy resources: A review," *Renewable and Sustainable Energy Reviews*, vol. 24, pp. 387–405, Aug. 2013.

[9] Y. Yusof, S. Sayuti, M. Latif, and M. Zamri, "Modeling and simulation of maximum power point tracker for photovoltaic system," *PECon 2004. Proceedings. National Power and Energy Conference, 2004.*, pp. 88–93, 2004.

[10] T. Morstyn, B. Hredzak, and V. G. Agelidis, "Distributed Cooperative Control of Microgrid Storage," *IEEE Transactions on Power Systems*, pp. 1–10, 2014.

[11] K. Le Dinh and Y. Hayashi, "Coordinated BESS control for improving voltage stability of a PV-supplied microgrid," in *2013 48th International Universities' Power Engineering Conference (UPEC)*, Sep. 2013, pp. 1–6.

[12] Xiaonan Lu, K. Sun, J. Guerrero, and J. . L. Vasquez, "SoC-Based Droop Method for Distributed Energy Storage in DC Microgrid Applications," in *2012 IEEE International Symposium on Industrial Electronics (ISIE)*, 2012, pp. 1640–1645.

[13] J. M. Guerrero, J. C. Vasquez, J. Matas, L. G. de Vicuna, and M. Castilla, "Hierarchical Control of Droop-Controlled AC and DC Microgrids-A General Approach Toward Standardization," *IEEE Transactions on Industrial Electronics*, vol. 58, no. 1, pp. 158–172, Jan. 2011.

[14] P.-H. Huang, W. Xiao, and M. El Moursi, "A Practical Load Sharing Control Strategy for DC Microgrids and DC Supplied Houses," in *Industrial Electronics Society, IECON 2013 - 39th Annual Conference of the IEEE*, 2013, pp. 7124 – 7128.

[15] K. Strunz, E. Abbasi, and D. N. Huu, "DC Microgrid for Wind and Solar Power Integration," *IEEE Journal of Emerging and Selected Topics in Power Electronics*, vol. 2, no. 1, pp. 115–126, Mar. 2014.

[16] Y. Gu, X. Xiang, W. Li, and X. He, "Mode-Adaptive Decentralized Control for Renewable DC Microgrid With Enhanced Reliability and Flexibility," *IEEE Transactions on Power Electronics*, vol. 29, no. 9, pp. 5072–5080, Sep. 2014.

[17] L. Xu and D. Chen, "Control and Operation of a DC Microgrid With Variable Generation and Energy Storage," *IEEE Transactions on Power Delivery*, vol. 26, no. 4, pp. 2513–2522, Oct. 2011.

[18] M. Noritake, K. Hirose, M. Yamasaki, T. Oosawa, and H. Mikami, "Evaluation results of power supply to ICT equipment using HVDC distribution system," in *Intelec 2010*. IEEE, Jun. 2010, pp. 1–8.

[19] D. Salomonsson, L. Soder, and A. Sannino, "An Adaptive Control System for a Dc Microgrid for Data Centers," in *2007 IEEE Industry Applications Annual Meeting*, vol. 44, no. 6, Sep. 2007, pp. 2414–2421.

[20] D. J. Hill, T. Liu, and G. Verbic, "Smart grids as distributed learning control," in *2012 IEEE Power and Energy Society General Meeting*, Jul. 2012, pp. 1–8.

[21] S. D. J. McArthur, E. M. Davidson, V. M. Catterson, A. L. Dimeas, N. D. Hatziargyriou, F. Ponci, and T. Funabashi, "Multi-Agent Systems for Power Engineering Applications-Part I: Concepts, Approaches, and Technical Challenges," *IEEE Transactions on Power Systems*, vol. 22, no. 4, pp. 1743–1752, Nov. 2007.

[22] V. Nasirian, S. Moayedi, A. Davoudi, and F. Lewis, "Distributed Cooperative Control of DC Microgrids," *IEEE Transactions on Power Electronics*, pp. 1–1, 2014.

[23] P.-H. Huang, P.-C. Liu, W. Xiao, and M. S. El Moursi, "A Novel Droop-Based Average Voltage Sharing Control Strategy for DC Microgrids," *IEEE Transactions on Smart Grid*, vol. 5, no. 5, pp. 1–1, Sep. 2014.

[24] C. Li, T. Dragicevic, N. L. D. Aldana, J. C. Vasquez, and J. M. Guerrero, "Voltage Scheduling Droop Control for State-of-Charge Balance of Distributed Energy Storage in DC Microgrids," in *Proceedings of the 2014 IEEE International Energy Conference (ENERGYCON)*, 2014.

[25] T. Morstyn, B. Hredzak, V. G. Agelidis, and G. Demetriades, "Cooperative control of DC microgrid storage for energy balancing and equal power sharing," in *2014 Australasian Universities Power Engineering Conference (AUPEC)*, no. October, Sep. 2014, pp. 1–6.

[26] J. W. Simpson-Porco, F. Dörfler, and F. Bullo, "Synchronization and power sharing for droop-controlled inverters in islanded microgrids," *Automatica*, vol. 49, no. 9, pp. 2603–2611, Sep. 2013.

[27] A. Bidram, A. Davoudi, F. L. Lewis, and J. M. Guerrero, "Distributed Cooperative Secondary Control of Microgrids Using Feedback Linearization," *IEEE Transactions on Power Systems*, vol. 28, no. 3, pp. 3462–3470, Aug. 2013.

[28] P. Sanchis, A. Ursaea, E. Gubia, and L. Marroyo, "Boost DC-AC Inverter: A New Control Strategy," *IEEE Transactions on Power Electronics*, vol. 20, no. 2, pp. 343–353, Mar. 2005.

[29] R. Olfati-saber, D. P. Spanos, and R. M. Murray, "Dynamic Consensus for Mobile Networks," in *2005 IFAC World Congress*, 2005.

[30] T. K. Refaat, R. M. Daoud, H. H. Amer, and E. A. Makled, "WiFi implementation of Wireless Networked Control Systems," in *2010 Seventh International Conference on Networked Sensing Systems (INSS)*, Jun. 2010, pp. 145–148.

[31] R. Olfati-Saber and R. Murray, "Consensus Problems in Networks of Agents With Switching Topology and Time-Delays," *IEEE Transactions on Automatic Control*, vol. 49, no. 9, pp. 1520–1533, Sep. 2004.

[32] Z. Yang, C. Shen, L. Zhang, M. Crow, and S. Atcitty, "Integration of a StatCom and battery energy storage," *IEEE Transactions on Power Systems*, vol. 16, no. 2, pp. 254–260, May 2001.

[33] B. Ryu, J. Kim, J. Choi, and C. Choi, "Design and analysis of output filter for 3-phase UPS inverter," in *Proceedings of the Power Conversion Conference-Osaka 2002 (Cat. No.02TH8579)*, vol. 3, 2002, pp. 941–946.

[34] R. Kuiava, R. A. Ramos, and N. G. Bretas, "Control design of a STATCOM with Energy Storage System for stability and power quality improvements," in *2009 IEEE International Conference on Industrial Technology*, Feb. 2009, pp. 1–6.

[35] Q. Shafiee, T. Dragicevic, J. C. Vasquez, and J. M. Guerrero, "Modeling, stability analysis and active stabilization of multiple DC-microgrid clusters," in *2014 IEEE International Energy Conference (ENERGYCON)*, May 2014, pp. 1284–1290.

[36] D. Chen, L. Xu, and L. Yao, "DC network stability and dynamic analysis using virtual impedance method," in *IECON 2012 - 38th Annual Conference of IEEE Industrial Electronics Society*, Oct. 2012, pp. 5625–5630.

[37] T. Tanaka, K. Hirose, D. Marquet, B. Sonnenberg, and M. Szpek, "Analysis of wiring design for 380-VDC power distribution system at telecommunication sites," in *Intelec 2012*, Sep. 2012, pp. 1–5.

[38] M. Villalva, J. Gazoli, and E. Filho, "Comprehensive Approach to Modeling and Simulation of Photovoltaic Arrays," *IEEE Transactions on Power Electronics*, vol. 24, no. 5, pp. 1198–1208, May 2009.


**Thomas Morstyn** (S'13) received the B.E. (Hon.) degree in electrical engineering from the University of Melbourne, Australia, in 2012.

He worked as an electrical engineer in the Rio Tinto Technology and Innovation group for two years. He is currently working towards the Ph.D. degree at the Australian Energy Research Institute, The University of New South Wales, Sydney, NSW, Australia. His current research interests include control systems for the integration of distributed renewable generation and storage into power networks.

**Branislav Hredzak** (M'98-SM'13) received the B.Sc./M.Sc. degree from the Technical University of Kosice, Slovak Republic, in 1993, and the Ph.D. degree from Napier University of Edinburgh, U.K., in 1997, all in electrical engineering.

He was a Lecturer and a Senior Researcher in Singapore from 1997 to 2007. He is currently a Senior Lecturer in the School of Electrical Engineering and Telecommunications, The University of New South Wales, Sydney, NSW, Australia. His current research interests include hybrid storage technologies and advanced control systems for power electronics and storage systems.

**Georgios D. Demetriades** (M'06) was born in Famagusta Cyprus. He received the M.Sc. degree in electrical engineering from the Democritus University of Thrace, Xanthi, Greece, and the Tech. Licentiate and Ph.D. degrees in power electronics from the Royal Institute of Technology (KTH), Stockholm, Sweden.

He worked in Cyprus for two years. In 1995, he joined ALSTOM Power Environmental Systems, Sweden. In 2000, he joined ABB Corporate Research, Västerås, Sweden, where he is currently a Research and Development Engineer. His current research interests include power electronics, voltage-source converter HVDC, flexible AC transmission system devices, high-frequency DC–DC power resonant converters, and high-frequency electromagnetic modelling.

**Vassilios G. Agelidis** (S'89-M'91-SM'00) was born in Serres, Greece. He received the B.Eng. degree in electrical engineering from the Democritus University of Thrace, Thrace, Greece, in 1988, the M.S. degree in applied science from Concordia University, Montreal, QC, Canada, in 1992, and the Ph.D. degree in electrical engineering from the Curtin University, Perth, WA, Australia, in 1997.

From 1993 to 1999, he was with the School of Electrical and Computer Engineering, Curtin University. In 2000, he joined the University of Glasgow, Glasgow, U.K., as a Research Manager for the Glasgow-Strathclyde Centre for Economic Renewable Power Delivery. In addition, he has authored/co-authored several journal and conference papers as well as Power Electronic Control in Electrical Systems in 2002. From January 2005 to December 2006, he was the inaugural Chair of Power Engineering in the School of Electrical, Energy, and Process Engineering, Murdoch University, Perth. From December 2006 to June 2010, he was the Energy Australia Chair of Power Engineering at the University of Sydney. He is currently the Director of the Australian Energy Research Institute, The University of New South Wales, Sydney, NSW, Australia.

Dr. Agelidis received the Advanced Research Fellowship from the United Kingdoms Engineering and Physical Sciences Research Council in 2004. He was the Vice President Operations within the IEEE Power Electronics Society during 2006-2007. He was an Associate Editor of the IEEE POWER ELECTRONICS LETTERS from 2003 to 2005, and served as the Power Electronics Society (PELS) Chapter Development Committee Chair from 2003 to 2005. He was an AdCom Member of IEEE PELS for 2007-2009 and the Technical Chair of the 39th IEEE Annual Power Electronics Specialists Conference, Rhodes, Greece.